re-BUŚ

Title: Studies of Deuteron Breakup Reactions in Deuteron–Deuteron Collisions at 160 MeV with BINA

Author: I. Ciepał, K. Bodek, N. Kalantar-Nayestanaki, G. Khatri, St. Kistryn, Barbara Kłos, Angelina Łobejko, Elżbieta Stephan, Andrzej Wilczek i in.

Citation style: Ciepał I., Bodek K., Kalantar-Nayestanaki N., Khatri G., Kistryn St., Kłos Barbara, Łobejko Angelina, Stephan Elżbieta, Wilczek Andrzej i in. (2019). Studies of Deuteron Breakup Reactions in Deuteron–Deuteron Collisions at 160 MeV with BINA. "Few-Body Systems" (Vol. 60 (2019), Art. No. 44), doi 10.1007/s00601-019-1510-3

UNIWERSYTET ŚLĄSKI W KATOWICACH   Biblioteka Uniwersytetu Śląskiego   Ministerstwo Nauki i Szkolnictwa Wyższego

I. Ciepał · K. Bodek · N.Kalantar-Nayestanaki ·
G. Khatri · St. Kistryn · B. Kłos · A. Kozela · J. Kuboś ·
P. Kulessa · A. Łobejko · A. Magiera · I. Mazumdar ·
J. Messchendorp · W. Parol · D. Rozpędzik ·
I. Skwira-Chalot · E. Stephan · A. Wilczek · B. Włoch ·
A. Wrońska · J. Zejma

Studies of Deuteron Breakup Reactions in Deuteron–Deuteron Collisions at 160 MeV with BINA

Abstract A rich set of differential cross section of the three-body ^{2}H$(d,dp)n$ breakup reaction at 160 MeV deuteron beam energy has been measured over a large range of the available phase space. The experiment was performed at KVI in Groningen, the Netherlands, using the BINA detector. The cross-section data for the breakup reaction have been normalized to the simultaneously measured ^{2}H$(d,d)^2$H elastic scattering cross section. The breakup cross sections obtained for 147 kinematically complete configurations near the quasi-free scattering kinematics are compared to the recent approximate calculations for the three-cluster breakup in deuteron–deuteron collisions. The cross sections for 294 kinematic configurations of the quasi-free scattering regime, for which no theoretical calculations exist, are also presented. Besides the three-body breakup, semi-inclusive energy distributions for the four-body ^{2}H$(d,pp)nn$ breakup are reported.

1 Introduction

Over the past 10 years, impressive progress has been made towards a numerical solution of the four-nucleon (4N) scattering problem. The complexity of 4N systems manifests itself in the existence of numerous resonances,

I. Ciepał (✉) · A. Kozela · J. Kuboś · W. Parol · B. Włoch · P. Kulessa
Institute of Nuclear Physics, PAS, 31342 Kraków, Poland
E-mail: izabela.ciepal@ifj.edu.pl

N. Kalantar-Nayestanaki · J. Messchendorp
KVI-CART, University of Groningen, 9747 AA Groningen, The Netherlands

K. Bodek · St. Kistryn · A. Magiera · D. Rozpędzik · A. Wrońska · J. Zejma
Institute of Physics, Jagiellonian University, 30348 Kraków, Poland

B. Kł os · A. Łobejko · E. Stephan · A. Wilczek
Institute of Physics, University of Silesia, 41500 Chorzow, Poland

G. Khatri
Department of Physics and Astronomy, Northwestern University, Evanston, IL 60208, USA

I. Skwira-Chalot
Faculty of Physics University of Warsaw, 02093 Warsaw, Poland

I. Mazumdar
Tata Institute of Fundamental Research, Mumbai 400 005, India

particularly in the low-energy region, a multitude of entrance and exit channels coupled with various total isospin states, and breakup thresholds at very low energies. In this respect, the 4N environment constitutes an auspicious, and because of the recent enormous progress in the calculations [1–8], attractive laboratory to study few-nucleon interaction models.

In the last 20 years, experimental physicists directed their efforts towards finding the effects of the three-nucleon force (3NF) in 3N systems [9–11]. In this case the exact calculations are performed with various so-called high-quality nucleon–nucleon (NN) potentials [12–14] with the use of the Faddeev equations [15]. They provide an almost perfect description of the NN data, but fail to describe the binding energies of 3N nuclei. The underbinding for the simplest 3N systems, Triton and ^{3}He, is around 0.8 MeV [16]. Another problem was found in proton–deuteron elastic scattering in the minimum of the differential cross section [17]. This proves that NN forces are not sufficient to describe even the most basic features of the 3N system. The existence of additional dynamics, 3NF, was proven by comparing precise data for 3N systems to state-of-the-art calculations. In general, including 3NF in the calculations improves the description of the cross-section data [10,11,18–26]. However, this claim is not necessarily true for the spin observables [19,20,24,27–30].

4N systems offer new possibilities to test nuclear interaction models and to learn about the isospin structure of 3NF [31]. Even more, they reveal extra sensitivity towards NN force models and can help understand the isospin symmetry of NN P-waves [32,33]. This, in turn, is important for solving the deuteron analyzing power puzzle or the space-star anomaly [9]. In 4N systems a larger sensitivity to the 3NF effects is expected, allowing the fine-tuning of the 3NF models. However, to get reliable information on the system dynamics, the experimental data need to be compared with accurate calculations. Such calculations involving 4N are mainly developed by three groups: Pisa [32,34] and Grenoble-Strasbourg [33,35], working in the coordinate-space representation, and the Lisbon–Vilnius group, using the momentum-space Alt–Grassberger–Sandhas (AGS) equations [36] for the transition operators [8]. All these methods include the Coulomb force, but only Lisbon–Vilnius calculates observables for multi-channel reactions above the breakup threshold [4–7].

Calculations for the *d-d* system at higher energies currently were feasible and were performed in the so-called single-scattering approximation (SSA) for the three-cluster breakup and elastic scattering [6]. This approximation is valid only near quasi-free scattering (QFS) kinematics (at the neutron spectator energy $E_n \sim 0$) at high-enough beam energies. A similar approximation was also used for three- and four-cluster breakups in the heavier system ^{12}C+p [37]. In the calculations three different 2N potentials were used: AV18 [12], CD Bonn [13] and CD Bonn+Δ [38]. In this approach the interaction was separated into two distinct contributions [6]. The first one, so-called one-term (*1-term*) of the single-scattering breakup amplitude, refers to a situation in which the target deuteron breaks up and only the interaction between the target proton and the deuteron beam is included. In this case the differential cross-section is peaked at the neutron spectator energy $E_n = 0$. The second one, so-called four term (*4-term*), refers to the other three SSA contributions related to the case in which the target proton does not interact (only the target neutron does) and a symmetric situation, but for the beam proton and beam neutron. These three cases together with the *1-term* are assigned to the *4-term* results. In the calculations the Coulomb force, interaction between *d-n* in *dp*-QFS and *d-p* in *dn*-QFS are neglected; therefore, the relative energy between *d-p* should be large enough to minimize the effects of the final state interactions. To demonstrate the reliability of the SSA calculations for the 4N system, the same kind of approximation was applied to the *p-d* breakup [6]. The exact calculations for the 3N breakup were compared to the ones obtained within SSA. The total *p-d* breakup cross-section calculated precisely is lower than the one obtained in SSA by 30% at 95 MeV and by 20% at 200 MeV. As the authors of Ref. [6] conclude, the recent theoretical predictions should give correct orders of magnitude for total and differential cross-sections for *d-d* and *p-d* breakup (near QFS) and elastic scattering.

With the two deuterons in the initial state, in addition to the simple elastic scattering process, several reactions with a pure hadronic signature can occur:

1. neutron-transfer: $d+d \rightarrow p+^3$H,
2. proton-transfer: $d+d \rightarrow n+^3$He,
3. three-body breakup: $d+d \rightarrow d+p+n$,
4. four-body breakup: $d+d \rightarrow p+p+n+n$.

The database is scarce for the elastic [39–43], breakup [44–49] and transfer channels [50–52]. In the breakup sector, the existing data were measured at low energies and only for very selected configurations. The new-generation data covering a large phase space were measured at KVI at 135 [43,53] and 160 MeV (this paper and

[54]). The data evaluation was focused on QFS, with the neutron acting as a spectator. The breakup analyzing power data for the ^{2}H(d,dp)n at 135 MeV were compared with elastic d-p scattering [43,53].

In this article, a set of differential cross section measured at 160 MeV deuteron beam energy for the three-body breakup is presented. The results obtained for the QFS geometries and their comparison to the recent SSA calculations [6] were already presented in Ref. [54]. Here, the cross-section integrated over energy (expressed in variable S) is shown. The database is supplemented with differential cross section for 294 kinematic configurations of the QFS regime, for which no theoretical calculations exist. Moreover, pilot studies of the four-body breakup ^{2}H(d,pp)nn are presented. In this case, two-dimensional correlations between the energies of the two protons are compared to the results of simulations.

2 Detector and Experimental Technique

BINA (Big Instrument for Nuclear Polarization Analysis) is a 4π detector which was designed to detect charged particles produced in reactions with hadrons at medium energies of up to 200 MeV/nucleon. BINA was installed at Kernfysisch Versneller Instituut (KVI) in Groningen, the Netherlands and operated at the superconducting cyclotron AGOR (Accelerator Groningen ORsay). The goal of the experiment at 160 MeV was to measure all the channels discussed above. In the experiment, the deuteron beam of very low current (about 5 pA) was impinging on a liquid deuterium target. Under such conditions the rate of accidental coincidences was minimized. The detector is divided into two main parts, the forward Wall and the backward Ball.

The forward Wall is composed of a three-plane Multi-Wire Proportional Chamber (MWPC), to reconstruct particles trajectories, and an array of ΔE-E telescopes to perform particle identification. The thick stopping E-detector, is used to measure the energy of particles. The forward Wall covers polar angles, θ, in the range of $10°$–$35°$ with the full range of azimuthal angles.

The backward Ball registers charged particles scattered at polar angles in the range of $40°$ to $165°$ with almost full azimuthal angle coverage. A detailed description of the BINA detection setup is presented in Refs. [52,55] and in the references cited therein.

3 Data Analysis

The main goal of the data analysis was to obtain a differential cross section for the ^{2}H(d,dp)n three-body breakup reaction, with special attention paid to the breakup configurations close to the quasi free scattering. However, a rich set of the cross sections for non-quasi-free geometries was also obtained and is presented in this paper. Besides the breakup cross sections, the differential cross section for d-d elastic scattering and the proton transfer channels were obtained [52]. All the cross-section data have been normalized relative to the existing data sets collected for the d-d elastic scattering at 180 and 130 MeV [41], see Refs. [52] for details.

The particles of interest (protons, deuterons and ^{3}He-ions) were identified using the ΔE-E technique. Graphical cuts selecting protons and deuterons were applied to the spectra for each ΔE-E telescope, whereas in the case of the ^{3}He-ions the so-called linearization method [52,56,57] was used. The breakup channel was analyzed with the requirement of proton–deuteron coincidences in the Wall. The two-body channels were identified on the basis of one particle registered in the Wall: the elastically-scattered deuterons or the ^{3}He-ions. The energy and efficiency calibrations were discussed in details in Refs. [52,54,55]. The energy calibration has been performed only for the thick, stopping E-detector. The lowest efficiency is related to the detection of particles in the MWPC. In the case of ΔE and E detectors, the efficiency is close to 100%. Corrections for losses due to the hadronic interactions inside the scintillator were also taken into account. The losses were calculated for protons, deuterons and ^{3}He-ions with the use of the GEANT4 framework and the results are presented in Fig. 1.

To check the GEANT4 simulations, elastic scattering events registered as Wall-Ball coincidences were used. Based on angular kinematical relations of the elastic scattering process, the events were selected with the requirement of coplanarity and correct correlation of θ polar angles. The particle identification was not applied since the events of interest are present in the tail of energy distributions, outside the deuteron identification cuts. In Fig. 2, the correlation of the energy deposited in the Wall scintillators at a forward angle of $\theta_{Wall} = 22°$ (which corresponds to 137 MeV deuteron energy) and in one of the phoswich detectors of the Ball ($\theta_{Ball} = 67.5°$) is presented.
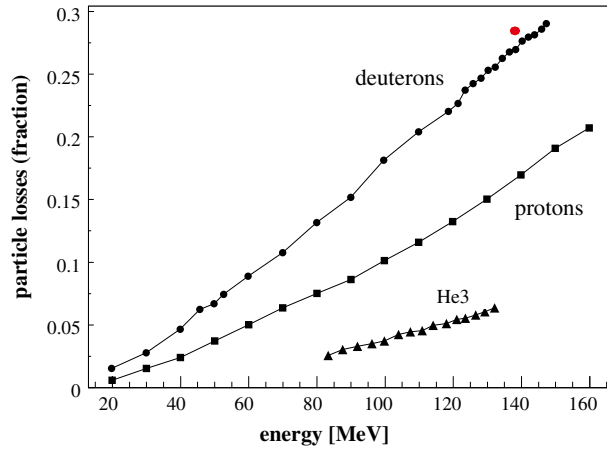
Fig. 1 (Color online) Relative loss of particles due to hadronic interactions in a plastic scintillator determined with using the GEANT4 Monte Carlo simulation package; the results are presented as a function of initial particle energy. The red dot represents the similar loss determined on the basis of the energy distribution of deuterons registered in this experiment, as shown in Fig. 2
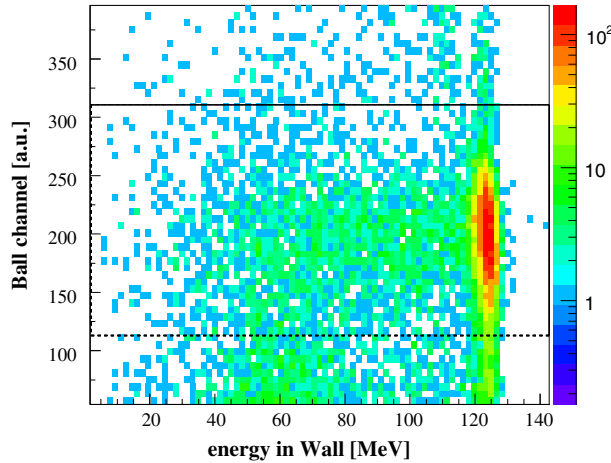

Fig. 2 The correlation between energies of particles registered in the Ball and Wall detectors which were selected based on the angular kinematical relations of the elastic scattering reaction. The peak corresponds to the elastically-scattered deuterons. The black frame refers to the selection of events used to calculate particle losses due to the hadronic interactions inside the Wall scintillators

The peak in Fig. 2 corresponds to the elastically-scattered deuterons and the tail stems from such deuterons undergoing hadronic interaction inside the scintillator. The losses calculated as a ratio of events in the tail to all events contained within the cut applied to the histogram are around 0.29 (Fig. 2), which agrees with the value of 0.27 obtained from the simulations.

The acceptance of the Wall for the registration of coincidences is limited by its granularity. When two particles hit the same slab of the E-detector or a strip of the ΔE-detector, their energies are not properly reconstructed and, as a consequence, such event is removed from the analysis. To establish the related efficiency (later referred to as configurational efficiency ε^{conf}), the $dp \rightarrow ppn$ breakup data collected with 160 MeV deuteron beam impinging on the proton target ([57,58]) were used. The deuteron–proton scattering has two advantages: *i)* only two channels are present: elastic scattering and *ppn* deuteron breakup, and *ii)* the cross section at the edges of kinematical curves is quite low. On the contrary, the *dpn* channel studied in this work is dominated by the quasi-free process in which the events are usually gathered on the edges of the kinematical curves (near detection thresholds). In view of the discussion below, this difference is quite crucial for determining configurational efficiency. The $dp \rightarrow ppn$ data were analyzed taking into account tracks that contain exactly two sets of *X-Y-U* hits in the three MWPC planes matching with a single *E*-bar (so-called *particular tracks*). Such events also include tracks with one particle stopped in ΔE or with a small energy deposit in the *E*-detector (below the threshold). To reject such events or minimize their impact, an upper limit

was set on the energy deposited in ΔE. Based on the *ppn* breakup, angular information from the MWPC (no PID available) and energy deposited in the ΔE-detector, the efficiencies were calculated for each geometrical configuration $(\theta_{p1}, \theta_{p2}, \varphi_{12})$ according to the formula:

$$\varepsilon^{conf}(\theta_{p1}, \theta_{p2}, \varphi_{pp}) = \frac{N_{break}(\theta_{p1}, \theta_{p2}, \varphi_{pp})}{N_{ce}(\theta_{p1}, \theta_{p2}, \varphi_{pp}) + N_{break}(\theta_{p1}, \theta_{p2}, \varphi_{pp})}, \tag{1}$$

where $N_{ce}(\theta_{p1}, \theta_{p2}, \varphi_{pp})$ denotes the number of *p-p* coincidences registered as the *particular tracks*, whereas $N_{break}(\theta_{p1}, \theta_{p2}, \varphi_{12})$ denotes number of the coincidences for the regular tracks. $N_{ce}(\theta_{p1}, \theta_{p2}, \varphi_{pp})$ and $N_{break}(\theta_{p1}, \theta_{p2}, \varphi_{pp})$ represent experimental values obtained by integrating the events over the arclength S (see Fig. 4). This procedure is also described in greater details in Ref. [54].

The corrections obtained from the data were also compared to the GEANT4 simulations. In the simulations, the uniform three-body breakup phase-space distribution has been used. The energy thresholds were also applied, similar to what is observed in the experimental data. The number of breakup coincidences was calculated and, simultaneously, the fraction of breakup coincidences with two particles registered in the same E or ΔE-detector, was obtained. In contrast to configurations characterized with the large relative azimuthal angle $\varphi_{dp} \geq 140°$, already discussed in Ref. [54], the ones with lower φ_{dp} values are more sensitive to efficiency losses due to *overlapping clusters* in the MWPC or double hits in the ΔE-strips. The cluster consists of a group of wires or a single wire that registers a signal in a given event. In the GEANT4 simulations of BINA the experimental distributions of cluster sizes in the MWPC were implemented, allowing the calculation of losses of events due to the *overlapping clusters*. In Fig. 3, examples of ε^{conf} determined on the basis of the data and the simulations are compared. By means of the simulations, one can investigate all the contributions of the efficiency separately for E, ΔE, and MWPC.

The ΔE and MWPC components play a role only at the lowest relative azimuthal angles φ_{dp}, while for the highest φ_{dp} only losses due to double hits in the E-detector contribute, see Fig. 3. The configurational efficiency calculated with the use of the simulations can be considered as purely geometrical. The statistical uncertainties are within 10%. The data and the simulations agree qualitatively, and usually the differences vary between 2% to 4% for the range of φ_{dp} above 120°, and reach up to 15% for several configurations characterized with the lowest φ_{dp}. These differences may lie in both: simulations and the experimental data. On one hand the simulations are rather simplified for not including data digitization and an ideal and realistic modeling of the detector geometry. On the other hand, the MWPC has its own configurational efficiency, which prevents the detection of two particles closer than some threshold distance (in each of three planes). Therefore, further analysis relies on the corrections for the double hits in the E and ΔE obtained directly from the experimental data and for the double hits in the MWPC based on the simulations.
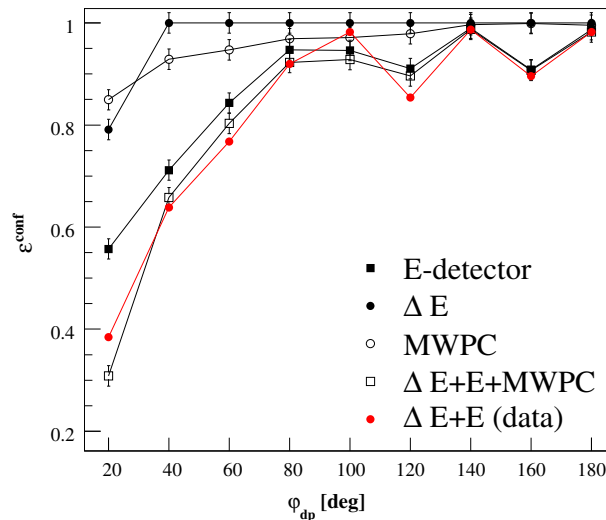

Fig. 3 (Color online) Configurational efficiency ε^{conf} for deuteron–proton coincidences calculated for configurations with $\theta_d = 18°$, $\theta_p = 18°$ from the data (red dots) and from the simulations (empty squares). Separate components of the inefficiency originating from double hits in the E-bars (black squares), ΔE-strips (black dots) or due to MWPC *overlapping clusters* (empty circles) are presented. Lines connecting points are used to guide the eye

4 Cross Section Normalization

The world d-d elastic scattering cross-section data [39–43,51], when presented as a function of four-momentum transfer $q = \mathbf{p}_d^{CM} \sqrt{\cos \theta_d^{CM} - 1}$, reveal very weak energy dependence in a certain range of q. Benefiting from this, the measured elastic scattering rate at 160 MeV was scaled to the data at two closest energies (130 and 180 MeV) [41] and the normalization factor κ was established [52,54]. Further, κ, corresponding to the luminosity integrated over the time of the data collection, was used to normalize cross sections for the $d+d \rightarrow$ $n+^3$He transfer [52] and breakup [54] reactions.

5 Differential Cross Section of $d+d \rightarrow d+p+n$ Breakup

The differential three-body breakup cross section was obtained for a set of geometrical configurations, defined by polar angles of deuteron (θ_d) and coincident proton (θ_p), and their relative azimuthal angle φ_{dp}.

The kinematical breakup spectra are presented in an E_p-E_d plane (energy of proton versus energy of deuteron), see Fig. 4, left panel. Two variables were introduced: D denoting the distance of the (E_d, E_p) point from the relativistic kinematics, and S, which defines the arc-length along the kinematics. The integration limits of $\Delta\theta_d = \Delta\theta_p = 2°$ and $\Delta\varphi_{dp} = 10°$ were used in a grid of θ_d, θ_p: $16° - 28°$, in steps of $2°$ and φ_{dp}: $20° - 180°$, in steps of $20°$. The events, corrected for efficiencies, were projected onto the D-axis in each bin of ΔS=4 MeV, see Fig. 4, right panel. To calculate the number of breakup events for a given S-bin, the Gauss function was fitted to the D-distributions. The background is mostly caused by hadronic interactions in the scintillator. Since the exact shape of the background is not known and its contribution is low (below 3%), as the first approximation linear behavior was assumed. To treat all the configurations consistently, the limits in the D variable were chosen at the values of D_a and D_b (see Fig. 4, right panel) corresponding to distances of -3σ and $+3\sigma$ from the maximum of the fitted peak.

The cross sections for geometries near the quasi-free-scattering (φ_{dp}: $140° - 180°$) are presented in the article [54]. In this paper, the cross sections for geometries away from the quasi-free-scattering region φ_{dp}: $20° - 120°$ (*non-quasi-free configurations*) are introduced. Sample cross-section distributions are presented for selected configurations in Figs. 5, 6, 7, 8, 9 and 10. The asymmetric systematic errors presented as red bands in Figs. 5, 6, 7, 8, 9 and 10 originate mostly from the track reconstruction procedure. The asymmetric errors, calculated for each individual configuration, were estimated based on three data sets obtained separately for three different methods of the track reconstruction, as was described in [54]. These uncertainties usually reach up to 7% and the maximum one is around 12%. Besides these uncertainties, other systematic errors (e.g. from normalization, background subtraction or calibration [54]) are taken into account and contribute to the bands. The total systematic uncertainty composed of systematic errors added in quadrature vary between 13 and 20%.
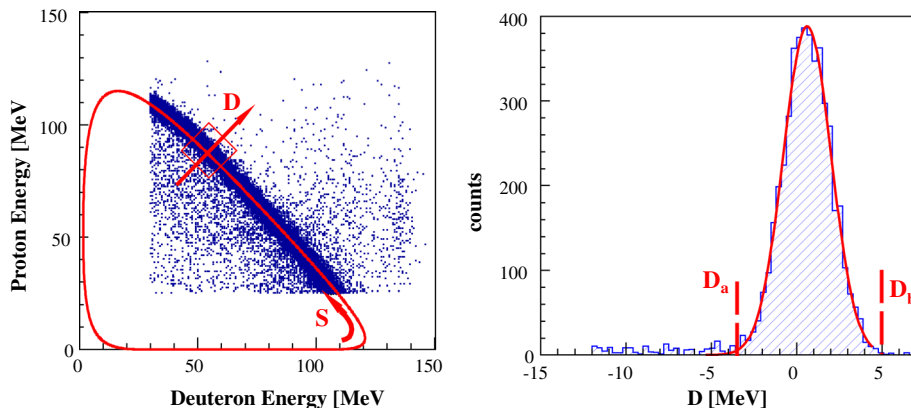

Fig. 4 (Color online) *Left panel:* E_p *vs.* E_d coincidence spectrum of the proton–deuteron pairs registered at $\theta_d = 18° \pm 1°$, $\theta_p = 22° \pm 1°$, $\varphi_{dp} = 120° \pm 5°$. The solid line shows a 3-body kinematical curve calculated for the central values of the angular ranges. Variables: arc-length S and distance from kinematics D are presented in a schematic way. *Right panel:* The projection of events belonging to one ΔS bin onto the D-axis. A Gaussian distribution was fitted in the range of D between D_a and D_b, corresponding to distances of -3σ and $+3\sigma$ from the fitted peak position
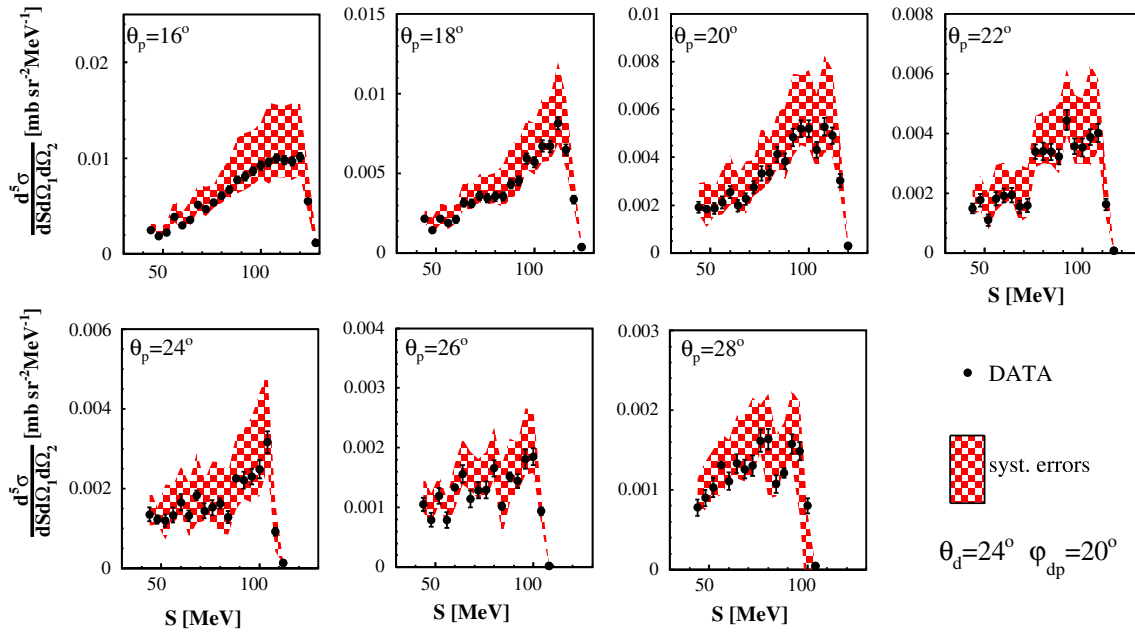
Fig. 5 Results at $\theta_d = 24°$ and $\varphi_{dp} = 20°$ for different θ_p (black points). The red bands represent systematic uncertainties
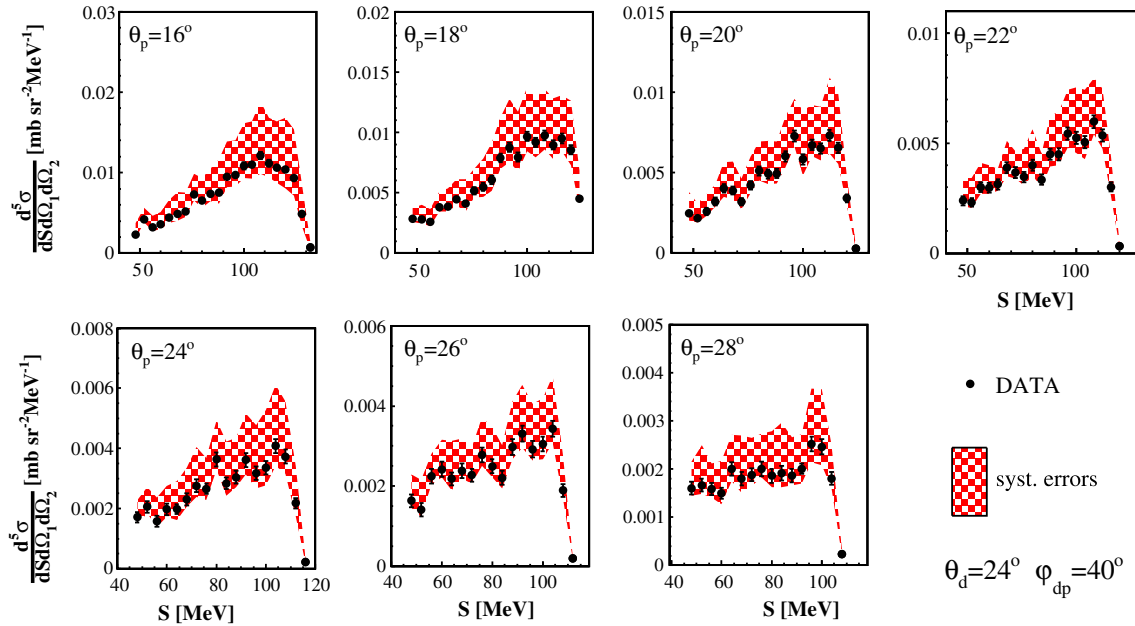

Fig. 6 Same as in Fig. 5, but for $\varphi_{dp} = 40°$

Currently, theoretical predictions are available only for configurations near the QFS region, in the so-called single-scattering approximation (SSA) for the three-cluster breakup [6], see also Sec. 1. The calculations were performed using the CD Bonn, AV18 and CD Bonn + Δ potentials in *1-* and *4-term* versions of the SSA calculations, see Fig. 11.

In the investigated phase-space region, corresponding to the forward part of the BINA setup, the breakup channel is dominated by the quasi-free scattering of the deuteron beam on proton from the deuteron target. The experimental cross sections were integrated over the S arc-length with the analogously treated theoretical predictions and are presented in Fig. 11. The cross section is strongly peaked in the region of quasi-free scattering and almost two orders of magnitude smaller for other geometries. The data were compared to the
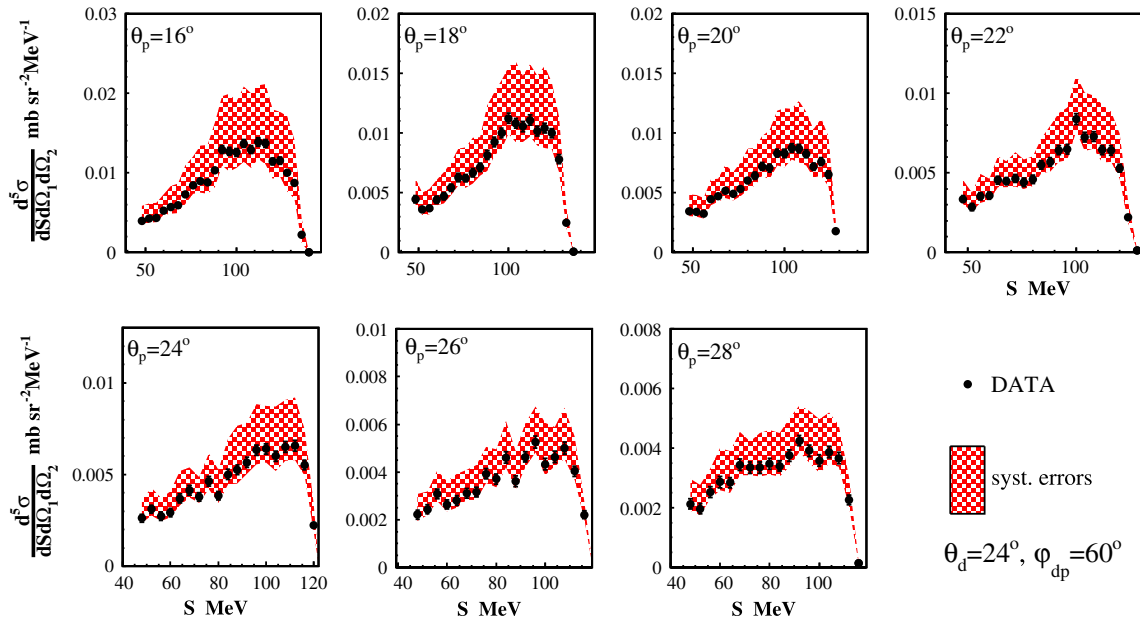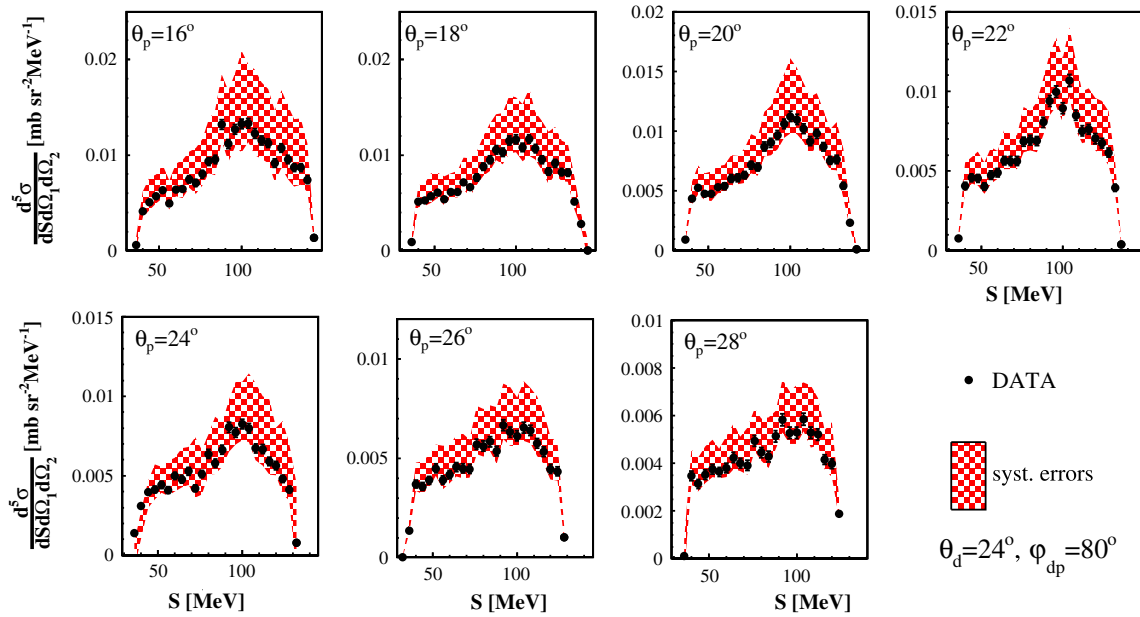
Fig. 7 Same as in Fig. 5, but for $\varphi_{dp} = 60°$

Fig. 8 Same as in Fig. 5, but for $\varphi_{dp} = 80°$

available SSA calculations at φ_{dp}=140°, 160° and 180°. Among the coplanar geometries, the ones with larger angles ($\theta_p \geq 24°$ and $\theta_d \geq 24°$) are better described by theory, as expected from SSA. Similar conclusions can be drawn for other (θ_p, θ_d) configurations, not shown in Fig. 11.

6 Four-Body Breakup $d+d \rightarrow p+p+n+n$

The exclusive measurement of the four-body *ppnn* breakup channel requires the detection of, at least, three particles. Within the BINA setup, this is very difficult due to the presence of two neutrons in the final state. The energies and scattering angles of both protons registered in the Wall can be precisely determined; however,
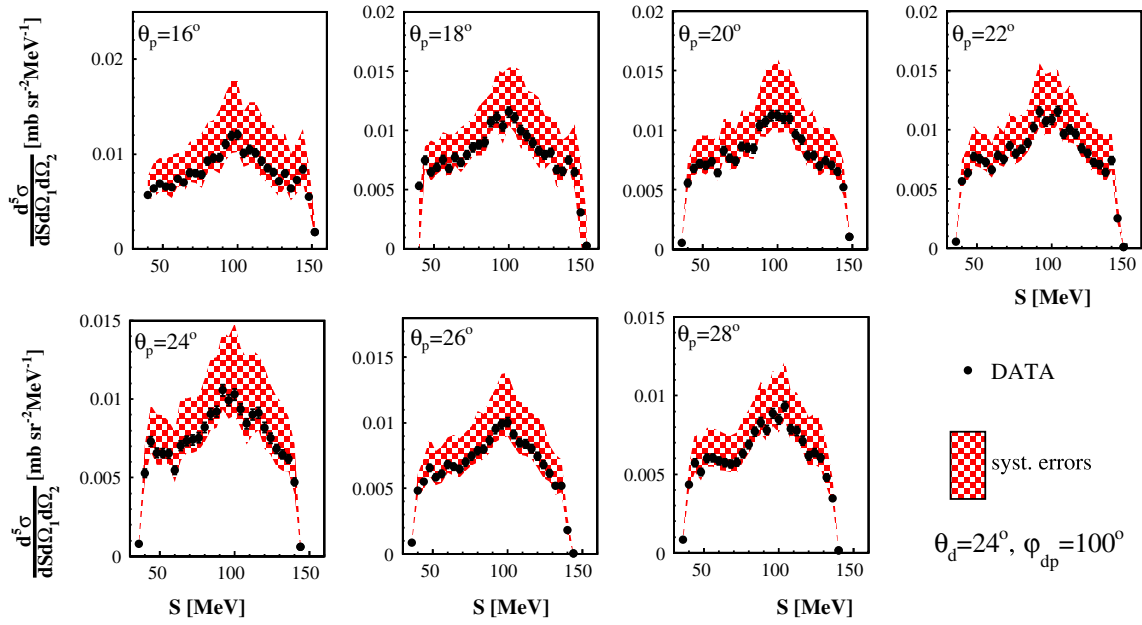
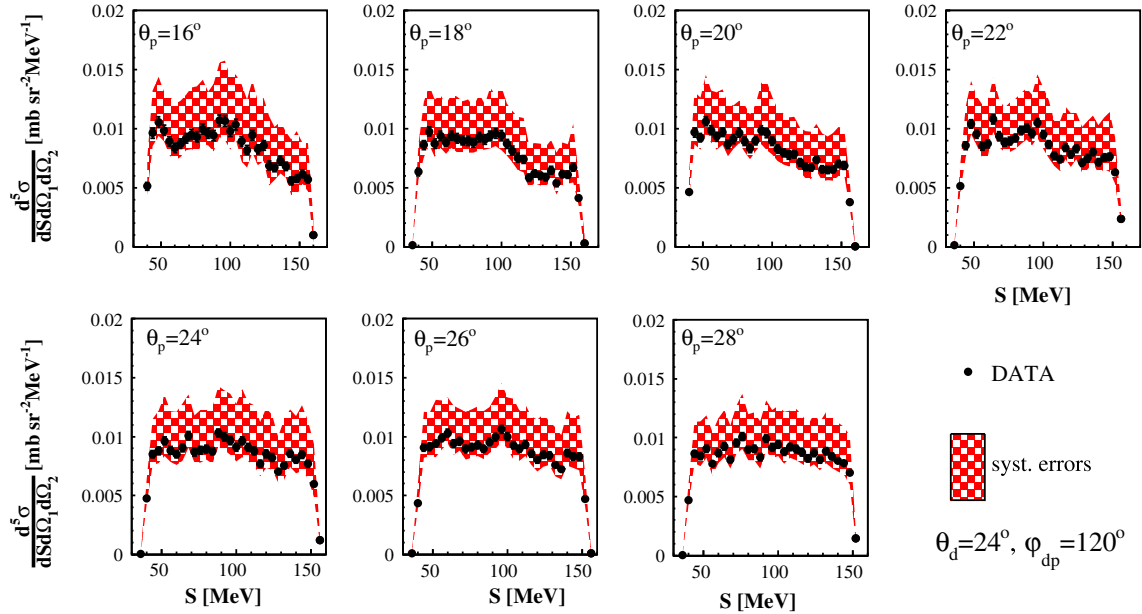**Fig. 9** Same as in Fig. 5, but for $\varphi_{dp} = 100°$

Fig. 10 Same as in Fig. 5, but for $\varphi_{dp} = 120°$

this is not sufficient. The complete kinematics can be established by measuring, in addition, the energy and the position of one of the neutrons. This is possible using the asymmetry of the signals registered in two PMTs (position along *E*-detector) and/or time-of-flight method (energy) [59]. The efficiency of registering three particles (*ppn*) in the Wall is significantly limited by the granularity of the detector. As discussed earlier, the configurational efficiency for double coincidences is strongly reduced in the case of triple coincidences. Therefore, semi-inclusive correlations between the energies of the two outgoing protons from the breakup have been investigated within the Wall acceptance. The correlations were drawn for the coplanar configurations of the two protons and compared to the results of simulations performed with the use of the Pluto++ event generator [60], see Fig. 12.
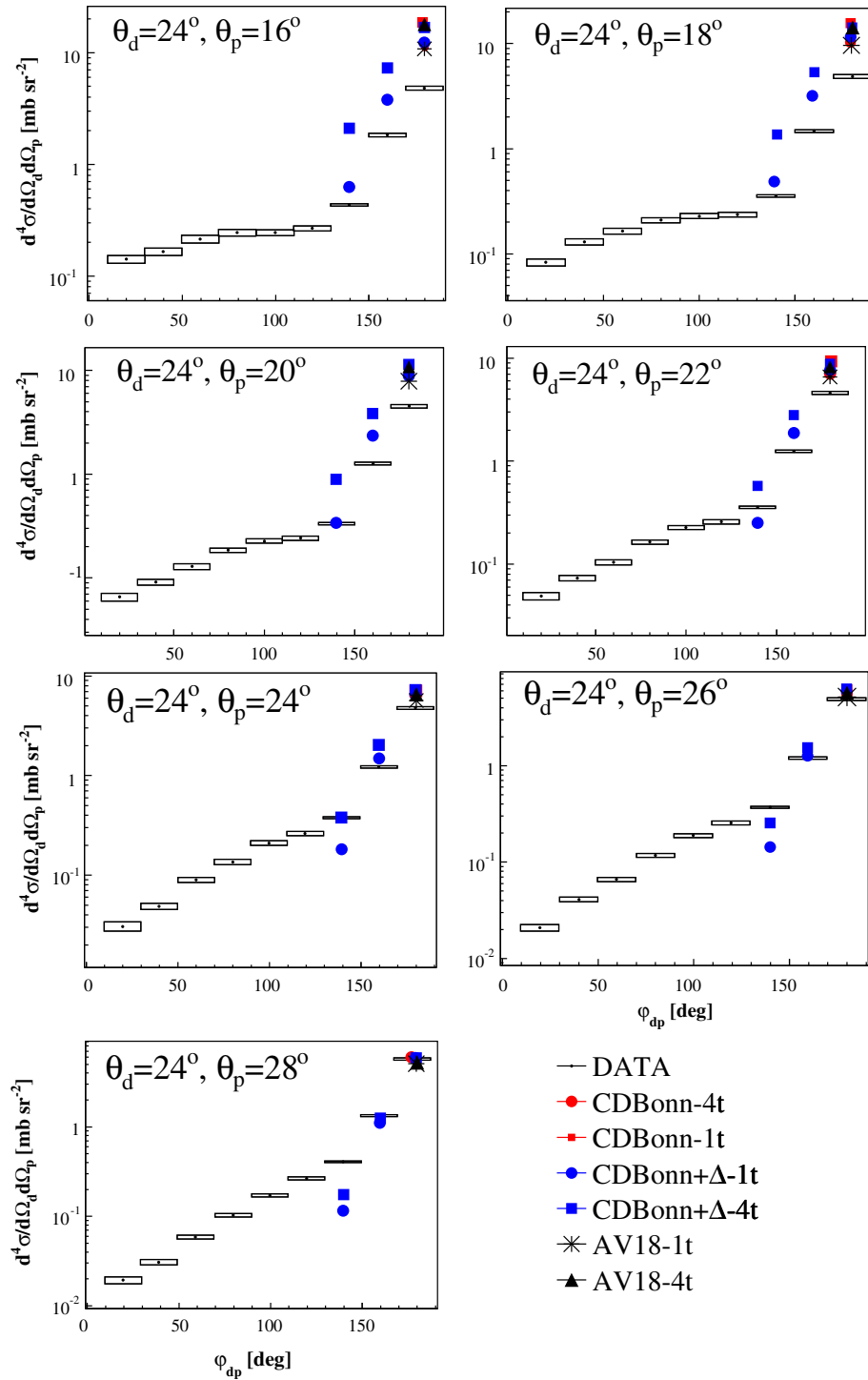
Fig. 11 Differential, integrated over S, cross section presented as a function of the relative azimuthal angle φ_{dp}, for pairs of the deuteron and proton polar angles θ_d, θ_p indicated in the panels. The data points are compared with the results of calculations based on pure CD Bonn, Argonne V18 and CD Bonn+Δ potentials for *1-term* (*1t*) and *4-term* (*4t*), as described in the legend. The boxes around the experimental points represent the systematic errors
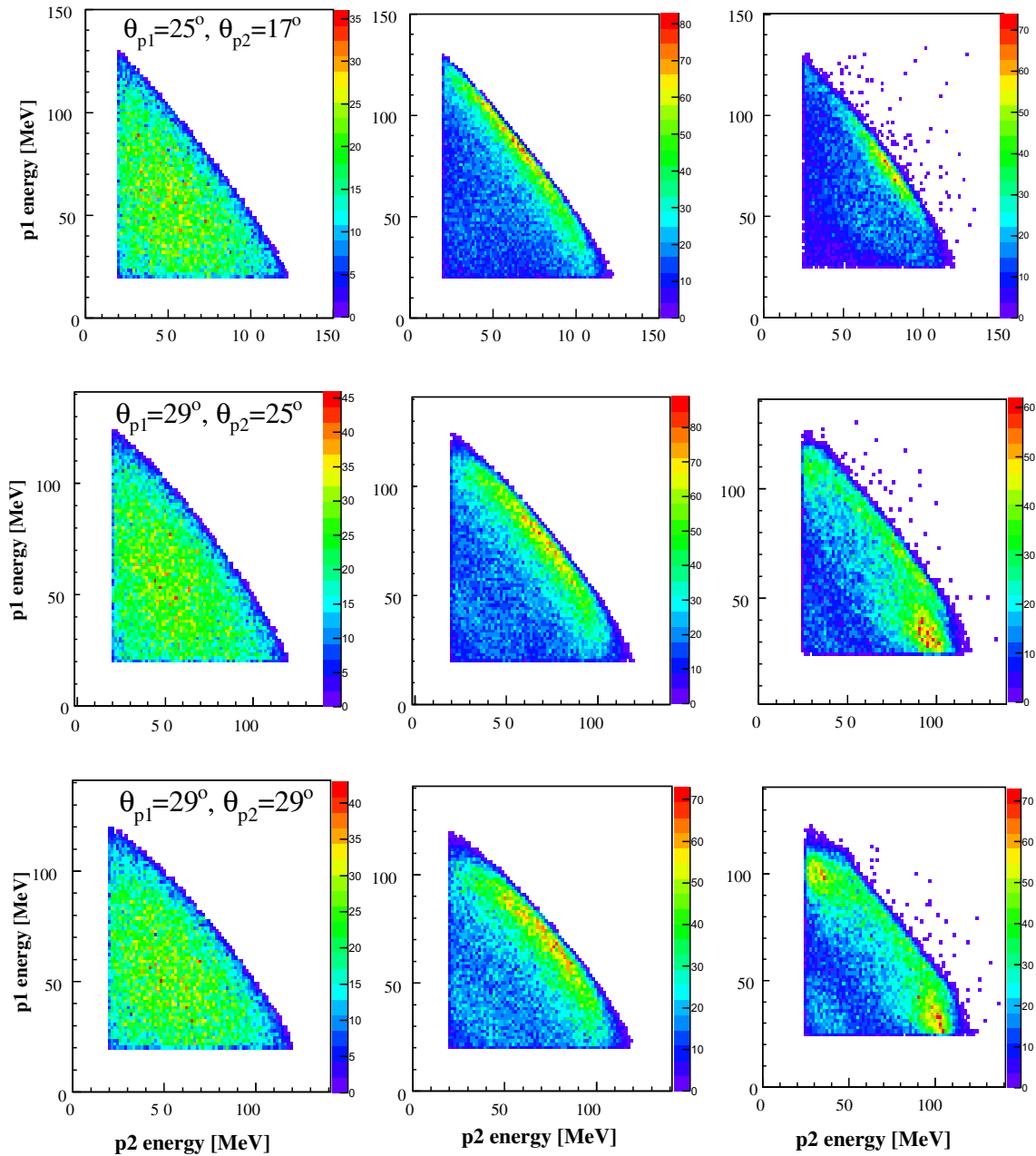
Fig. 12 (Color online) The correlation between the energies of the two protons in the deuteron–deuteron four-body breakup are shown for the three coplanar configurations ($\varphi_{pp} = 180°$) presented in the panels. In the left and center columns, results of the simulations are shown for *ppnn* and *ppnn$_{spec}$* respectively. In the right column similar correlations, but for the data are presented

An inclusive analysis introduces integration over certain variables; therefore, the Monte Carlo simulations make important contributions to the interpretation of the data. Due to the lack of theoretical calculations, the pilot simulations have been performed based on the phase space or on the simplified QFS modeling. By comparing the data with the simulations one can identify patterns related to QFS or to the dynamics beyond these assumptions.

In Pluto++ the quasi-free scattering of a nucleon N_1 on a nucleus A (or vice versa) is accomplished in two steps: first, the Fermi-momentum and off-shell mass of the nucleon N_1 inside the nucleus A are determined and the particle properties are set up accordingly, and in a second step the reaction $N_1 + N_2$ is performed. At the moment a dedicated sampling model is included for the deuteron wave function [61].

The simulations have been performed for two cases. Events have been generated according to the uniform four-body breakup phase-space ($ppnn$) and, in the second case, using the quasi-free scattering model, with one of the neutron being a spectator ($ppnn_{spec}$). Then, the charged particles were tracked through the BINA detector using the dedicated GEANT4 simulations. In Fig. 12, left and middle columns, results of the simulations are presented for three different proton-proton coplanar configurations ($\varphi_{pp} = 180°$): (θ_p, θ_p)=(25°, 17°), (29°, 17°) and (29°, 29°). The distributions were compared to the similar experimental spectra, see Fig. 12, right column. The experimental distributions reveal that structures ("blobs"), when compared with results of simulations presented in the middle column, can be interpreted as a contribution of QFS (with the target neutron as a spectator) and strong *p-n* final state interaction. Similar structures are also visible in the *ppn* breakup measured at the same deuteron beam energy [57,58] and in the same configurations as presented in Fig. 12.

7 Summary and Outlook

The ^{2}H(*d, dp*)*n* breakup reaction was studied with the BINA setup covering a large part of the phase space. These investigations allow for a systematic analysis of the cross-section data. The database for the three-body breakup has been significantly enriched with 441 proton–deuteron configurations at 160 MeV deuteron beam energy. The cross sections have been compared to the calculations based on the single-scattering approximation, which are applicable only near the QFS region and at higher energies [6]. The calculations are not exact, but they provide the correct order of magnitude for the cross sections. The cross sections calculated in SSA are higher than the experimental ones, which are expectedly based on the comparison between the breakup cross sections calculated in an exact way and the one obtained in SSA. This is also true for the results presented in this paper.

The development of models involving 4N systems is ongoing; however, exact numerical calculations for breakup amplitudes are still distant in time given the complexity of the problem. Current experimental efforts are focused on the further development of the 4N database with the aim of building the testing ground for future calculations.

References

1. A. Deltuva, A.C. Fonseca, P.U. Sauer, Phys. Lett. **B660**, 471 (2008)
2. A. Deltuva, A.C. Fonseca, Phys. Rev. **C87**, 054002 (2013)
3. A. Deltuva, A.C. Fonseca, Phys. Rev. **C90**, 044002 (2014)
4. A. Deltuva, A.C. Fonseca, Phys. Rev. **C92**, 024001 (2015)
5. A. Deltuva, A.C. Fonseca, Phys. Lett. **B742**, 285 (2015)
6. A. Deltuva, A.C. Fonseca, Phys. Rev. **C93**, 044001 (2016)
7. A. Deltuva, A.C. Fonseca, Phys. Rev. **C95**, 024003 (2017)
8. A.C. Fonseca, A. Deltuva, Few-Body Syst. **58**, 46 (2017)
9. K. Sagara et al., Few-Body Syst. **48**, 59 (2010)
10. N. Kalantar-Nayestanaki et al., Rep. Prog. Phys. **75**, 016301 (2012)
11. St Kistryn, E. Stephan, J. Phys. G Nucl. Part. Phys. **40**, 063101 (2013)
12. R.B. Wiringa, V.G.J. Stoks, R. Schiavilla, Phys. Rev. **C51**, 38 (1995)
13. R. Machleidt, Phys. Rev. **C63**, 024001 (2001)
14. V.G.J. Stoks et al., Phys. Rev. **C49**, 2950 (1994)
15. L.D. Faddeev, Sov. Phys. JETP **12**, 1014 (1961)
16. R.B. Wiringa, A.R. Smith, T.L. Ainsworth, Phys. Rev. **C29**, 1207 (1984)
17. H. Shimizu et al., Nucl. Phys. **A382**, 242 (1982)
18. K. Ermish et al., Phys. Rev. Lett. **86**, 5862 (2001)
19. K. Ermish et al., Phys. Rev. **C68**, 051001 (2003)
20. K. Ermish et al., Phys. Rev. **C71**, 064004 (2005)
21. St Kistryn et al., Phys. Rev. **68**, 054004 (2003)

22. St Kistryn et al., Phys. Rev. **C72**, 044006 (2005)
23. M. Kistryn et al., Phys. Lett. **B641**, 23 (2006)
24. H. Sakai et al., Phys. Rev. Lett. **84**, 5288 (2000)
25. K. Sekiguchi et al., Phys. Rev. Lett. **95**, 162301 (2005)
26. I. Ciepał et al., Few-Body Syst. **56**, 665 (2015)
27. K. Sekiguchi et al., Phys. Rev. **C70**, 014001 (2004)
28. E. Stephan et al., Phys. Rev. **C82**, 014003 (2010)
29. E. Stephan et al., Eur. Phys. J. Appl. Phys. **A49**, 36 (2013)
30. R. Bieber et al., Phys. Rev. Lett. **84**, 606 (2000)
31. H. Mardanpour et al., Phys. Lett. **B687**, 149 (2010)
32. M. Viviani, L. Girlanda, A. Kievsky, L.E. Marcucci, Phys. Rev. Lett. **111**, 172302 (2013)
33. R. Lazauskas, J. Carbonell, Phys. Rev. **C79**, 054007 (2009)
34. A. Kievsky et al., J. Phys. **G35**, 063101 (2008)
35. R. Lazauskas, J. Carbonell, Phys. Rev. **C70**, 044002 (2004)
36. E.O. Alt, P. Grassberger, W. Sandhas, Phys. Rev. **C1**, 85 (1967)
37. A. Deltuva, Phys. Rev. **C87**, 034609 (2013)
38. A. Deltuva, R. Machleidt, P.U. Sauer, Phys. Rev. **C68**, 024005 (2003)
39. A. Micherdzińska et al., Phys. Rev. **C75**, 54001 (2007)
40. C. Alderliesten, A. Djaloeis, Phys. Rev. **C18**, 2001 (1978)
41. C. Bailey, Ph. D. thesis, Indiana University, U.S.A., (2009)
42. A. Ramazani-Moghaddam-Arani, Ph.D. thesis, University of Groningen, (2009)
43. A. Ramazani-Moghaddam-Arani et al., Phys. Rev. **C83**, 024002 (2011)
44. V. Valković et al., Nucl. Phys. **A183**, 126 (1972)
45. A.A. Cowley et al., Nucl. Phys. **A220**, 429 (1974)
46. H. Yuasa, Suppl. Prog. Theor. Phys. **61**, 161–179 (1977)
47. W. Kluge et al., Nucl. Phys. **A302**, 93 (1978)
48. B.J. Wielinga et al., Nucl. Phys. **A383**, 11 (1981)
49. L.T. Myers et al., Phys. Rev. **C28**, 29 (1983)
50. M. Roy et al., Phys. Lett. **B29**, 2 (1969)
51. G. Bizard et al., Phys. Rev. **C22**, 1632 (1980)
52. I. Ciepał et al., Phys. Rev. **C99**, 014620 (2019)
53. A. Ramazani-Moghaddam-Arani et al., Phys. Lett. **B725**, 282 (2013)
54. I. Ciepał et al., arXiv:1901.10737 [nucl-ex]
55. G. Khatri, Ph.D. thesis, Jagiellonian University, Kraków, (2015)
56. J. Płoskonka et al., Nucl. Instrum. Methods Phys. Res. **126**, 57 (1975)
57. W. Parol et al., EPJ Web Conf. **81**, 06007 (2014)
58. W. Parol et al., Acta Phys. Pol. **B10**, 149 (2017)
59. B. Włoch et al., Acta Phys. Pol. **B49**, 445 (2018)
60. I. Fröhlich, PoS ACAT2007:076, (2007). https://doi.org/10.22323/1.050.0076
61. P. Benz et al., Nucl. Phys. **B65**, 158 (1973)